MOLECULAR AND CELLULAR BIOLOGY, Sept. 2005, p. 7758–7769 Vol. 25, No. 17
0270-7306/05/$08.00+0 doi:10.1128/MCB.25.17.7758–7769.2005

Manganese Superoxide Dismutase Induces p53-Dependent Senescence in Colorectal Cancer Cells

Lars Behrend,[1] Andrea Mohr,[2] Tatjana Dick,[1] and Ralf M. Zwacka[1]*

Division of Gene Therapy, University of Ulm, 89081 Ulm, Germany,[1] and National Centre for Biomedical Engineering Science, National University of Ireland Galway, Galway, Ireland[2]

Received 21 September 2004/Returned for modification 5 November 2004/Accepted 3 June 2005

The mitochondrial enzyme manganese superoxide dismutase (MnSOD) is known to suppress cell growth in different tumor cell lines. However, the molecular mechanism of this growth-retarding effect is not fully understood. Here we show that overexpression of MnSOD slows down growth of HCT116 human colorectal cancer cells by induction of cellular senescence. MnSOD overexpression causes up-regulation of p53 and its transcriptional target, the cyclin-dependent kinase inhibitor p21. Adenovirus-mediated knockdown of p53 by RNA interference rescues MnSOD-overexpressing clones from growth retardation. Accordingly, the overexpression of MnSOD in HCTp53$^{-/-}$ cells does not lead to senescence, whereas in HCTp21$^{-/-}$ cells we found induction of senescence by forced expression of MnSOD. These results indicate a pivotal role of p53, but not p21, in the observed effects. Analysis of the mitochondrial membrane potential revealed reduced polarization in MnSOD-overexpressing cells. In addition, depolarization of the mitochondrial membrane by mitochondrial inhibitors such as rotenone or antimycin A led colorectal cancer cells into p53-dependent senescence. Our data indicate that uncoupling of the electrochemical gradient by increased MnSOD activity gives rise to p53 up-regulation and induction of senescence. This novel mitochondrially mediated mechanism of tumor suppression might enable strategies that allow reactivation of cellular aging in tumor cells.

Most types of primary mammalian cells have a limited proliferative life span, i.e., after a finite number of cell cycles, cells become unable to enter S phase in response to mitogenic stimulation (4). This growth blockade has been termed "replicative senescence" and is accompanied by specific morphological alterations such as increased cell size and flattening of the cytoplasm. Cancer cells can escape this cell fate by entering an immortalized cellular program. Therefore, recent research efforts have concentrated on how transformed cells overcome this senescence proliferative barrier.

Besides replicative senescence, an acute and inducible form of senescence has been described that can be triggered in response to chemotherapeutic drugs in lymphomas (35) as well as in solid tumors (41). Tumor suppressors such as p53, Rb, or $p16^{INK4A}$ (10, 15, 19) have been identified as important activators of senescence (23, 35, 37, 47). In viral transformation, the inactivation of viral oncoproteins which act through the p53/Rb pathway, such as the simian virus 40 large-T antigen or human papillomavirus protein E6 or E7, leads to the induction of cellular senescence (14, 31, 47). Mutational loss of senescence inducers has been shown to reduce chemotherapeutic responsiveness and also to correlate with poor prognosis (34).

Beyond the stress induced by up-regulation of tumor suppressors, "oncogenic stress," i.e., the inappropriate activation of oncogenes such as Ras or c-Myc, can result in senescence. In primary human cells (4, 36) and in mouse keratinocytes (42), Ras activation leads to premature senescence. Interestingly, the tumor suppressor and oncogene pathways seem to cooperate in senescence induction. In murine fibroblasts, activation of the mitogen-activated protein kinase pathway by oncogenic Ras converts p53 into an inducer of $p19^{ARF}$-dependent senescence (12). Hence, while normal cells implement a fail-safe mechanism against excessive mitogenic stimulation by induction of senescence, malignant cells bypass the onset of senescence due to the inactivation of tumor suppressors.

Induction of mitogenic signaling through the Ras/Rac pathway induces the formation of reactive oxygen species (ROS) (16), and an elevated oxidative status is indispensable for mitogenic stimulation. Accordingly, chemical and enzymatic antioxidants have been shown to suppress tumor cell growth (21, 27). A potent antioxidant enzyme in suppressing cell growth in a variety of cancer cell lines (22, 24, 48) and in mouse models (20, 30) is the manganese superoxide dismutase (MnSOD). MnSOD is a mitochondrial matrix protein that catalyzes the dismutation of superoxide radicals ($O_2\cdot^-$) to hydrogen peroxide (H_2O_2). However, the signaling pathways regulated by antioxidant enzymes such as MnSOD that contribute to growth retardation of cancer cells have yet to be elucidated in detail.

We show that overexpression of MnSOD in the colon cancer cell line HCT116, which harbors wild-type p53, provokes a senescence-associated growth arrest. Using p53 and p21 isogenic knockout cell lines (HCTp53$^{-/-}$ and HCTp21$^{-/-}$) and RNA interference (RNAi), we found p53, but not p21, to be required for this acute senescence phenotype. Our observations imply that the MnSOD growth-retarding functions are at least partially due to triggering of a p53-dependent cellular senescence program. We show that MnSOD-mediated decreases in mitochondrial membrane polarization lead to p53 activation. Elucidation of the molecular events that lead from p53 to senescence may provide avenues to reinstate this cellu-

* Corresponding author. Mailing address: University of Ulm, Division of Gene Therapy, Helmholtzstr. 8/1, 89081 Ulm, Germany. Phone: (49731) 50033617. Fax: (49731) 50033609. E-mail: ralf.zwacka@medizin.uni-ulm.de.

lar response in tumor cells harboring mutant, dysfunctional p53.

MATERIALS AND METHODS

Cell lines and stable transfection. The parental colon cancer cell line HCT116 and the p53- and p21-null clones HCTp53$^{-/-}$ and HCTp21$^{-/-}$ (2), respectively, derived by homologous recombination, were a generous gift from B. Vogelstein (Howard Hughes Medical Institute, The Johns Hopkins Oncology Center). The cells were cultured in McCoy's medium supplemented with 10% fetal calf serum (FCS) and 1% penicillin-streptomycin. HCT*MnS*, HCTp53$^{-/-}$*MnS* (referred to below as p53$^{-/-}$*MnS*), and HCTp21$^{-/-}$*MnS* (referred to below as p21*MnS*$^{-/-}$) cell lines were established by stable transfection of pcDNA3.1-MnSOD, which contains the human sequence of MnSOD, together with the pSV.puro vector and subsequent selection with 2.5 μg/ml puromycin. For maintenance of established clones, we used 0.5 μg/ml puromycin. All assays were performed in medium without puromycin. Homogeneity in transgene expression was achieved by subcloning MnSOD-overexpressing cell lines in 96-well plates. MnSOD expression was determined by Western blot analysis. Clones that were solely transfected with pSV.puro were isolated and compared to their parental HCT116, HCTp53$^{-/-}$, and HCTp21$^{-/-}$ cells, respectively. These pSV.puro clones did not differ in growth behavior, senescence, or mitochondrial membrane potential (MMP) from their parental cells.

Reagents and antibodies. Unless otherwise stated, all reagents were purchased from Sigma. Antimycin A (AA) was stored at −20°C as a 40 mM stock solution in methanol, while rotenone (ROT) was dissolved in dimethyl sulfoxide and stored as a 10 mM stock solution at −20°C. Antibodies used in the present study were as follows: rabbit polyclonal anti-MnSOD (StressGene), sheep polyclonal anti-copper, zinc superoxide dismutase (anti-CuZnSOD) (The Binding Site), mouse monoclonal anti-p53 (DO-1) (BD PharMingen), mouse monoclonal anti-p21 (BD PharMingen), and goat polyclonal anti-actin (I-19) (Santa Cruz).

Western blotting. Cells were washed in ice-cold phosphate-buffered saline (PBS) and harvested, and cell pellets were extracted for 40 min with lysis buffer (50 mM Tris-HCl [pH 8.0], 150 mM NaCl, 10% glycerol, 1 mM dithiothreitol, 1 mM EDTA, 1% NP-40, proteasome inhibitor cocktail-1 [1:2,500]) on ice. Extracts were cleared by centrifugation for 15 min at 12,000 × *g* at 4°C. After determination of protein concentrations, samples were denatured in sample buffer (1% sodium dodecyl sulfate [SDS], 0.1% bromophenol blue, 10% glycerol), separated on SDS-polyacrylamide gels, and transferred to a nitrocellulose membrane (Hybond-ECL; Amersham). The membranes were blocked for 1 h in blocking buffer (3% nonfat dry milk solution and 0.1% Tween 20 in PBS) and subsequently probed with the indicated primary antibodies in blocking buffer for 1 h. After three washing steps in wash buffer (0.1% Tween 20 in PBS), the blots were subjected to secondary horseradish peroxidase-conjugated anti-rabbit (Amersham), anti-mouse (Amersham), or anti-goat/sheep (Sigma) antibodies for 45 min in blocking buffer. After three washing steps in PBS–0.1% Tween 20, proteins were visualized by chemiluminescence detection (ECL solutions; Amersham).

Northern blotting. RNA was isolated with the RNeasy purification kit (QIAGEN) according to the manufacturer's protocol. For each sample, 15 μg of RNA was incubated at 65°C for 10 min with ethidium bromide and loading buffer (5% glycerol, 1 mM EDTA, 0.4 mg/ml bromophenol blue) and separated on a formaldehyde-agarose gel (1% agarose, 6% formaldehyde) in morpholinepropanesulfonic acid (MOPS) running buffer (200 mM MOPS, 50 mM sodium acetate, 10 mM EDTA, pH 7.0). After RNA transfer to a Hybond-N membrane (Amersham) by capillary blotting overnight, the membrane was prehybridized in Denhardt's hybridizing buffer (2% polyvinylpyrrolidone, 2% bovine serum albumin, 2% Ficoll-400) for at least 60 min at 42°C. Hybridization with the radioactive probe was carried out overnight in hybridizing buffer (5× SSC [1× SSC is 150 mM NaCl plus 15 mM sodium citrate, pH 7.0], 50% formamide, 5× Denhardt's buffer, 1% SDS, 10% dextrane sulfate) at 42°C. The p53 probe was generated by PCR using the forward primer 5′-CATGTGTAACAGTTCCTGCAT-3′ and the reverse primer 5′-TCATTCAGCTCTCGGAACATCTC-3′. The PCR fragments were gel purified and labeled using a Readiprime II random prime kit (Amersham) before they were purified using Sephadex G25 columns (Amersham). Following hybridization, membranes were washed with 2× SSC–0.1% SDS first for 15 min at room temperature and subsequently for 45 min at 65°C before the signals were visualized on X-ray film.

Measurement of apoptosis. Determination of apoptotic cells in untreated cultures of HCT116 and HCT*MnS*9 was performed according to a protocol of Nicoletti and coworkers (28). Cells were harvested, washed, and stained overnight in a buffer containing propidium iodide and 0.5% Triton X-100. After incubation at 4°C for 16 h, 6,000 cells were analyzed by flow cytometry (Becton Dickinson; FACSCalibur) in the Fl-3 channel on a logarithmic scale, and sub-G_1 cells were counted as apoptotic.

Determination of cellular senescence. The state of cellular senescence was determined by senescence-associated β-galactosidase (SA-β-Gal) staining at pH 6.0 according to the protocol of Dimri and coworkers (9). After staining for 16 to 24 h at room temperature, micrographs were taken from cell culture dishes or from embedded samples. In addition, we measured the DNA synthesis rate by cytometric analysis of bromodeoxyuridine (BrdU) incorporation. The experiment was performed according to the manufacturer's protocol (Roche). Briefly, cells were harvested after a 30-min pulse with BrdU in the medium and were treated with HCl. After incubation with a fluorescein isothiocyanate-coupled anti-BrdU antibody, cells were washed and incubated with 20 μg/ml propidium iodide in PBS before flow cytometric analysis.

Immunofluorescence microscopy. All steps were carried out at room temperature. Cells were grown on glass coverslips. For fixation, cells were incubated in 3% paraformaldehyde–PBS for 15 min, washed twice in PBS, and permeabilized for 5 min in 0.3% Triton X-100–PBS. After two washing steps with PBS, the samples were blocked in PBS containing 1% FCS for 60 min, followed by incubation steps with a primary anti-p53 (Do-1) antibody for 45 min and a rhodamine-conjugated secondary anti-mouse antibody (Dianova) for 30 min in PBS. Epifluorescence microscopic pictures were taken on a Zeiss Axiovert 135 microscope equipped with a 14-bit digital camera (Axiocam; Zeiss) and the camera software Axiovision 3.0 (Zeiss).

Adenovirus production and transduction. Recombinant E1-deleted adenovirus vectors were generated using the ViraPower adenovirus expression system (Invitrogen) and produced as previously described (52). Adenovirus vectors Ad.shRNA.p53 and Ad.shRNA.EGFP encoded small hairpin RNA (shRNA) constructs targeted against the p53 (1) and jellyfish enhanced green fluorescent protein (EGFP) genes, respectively, under the control of the human U6 promoter. Purified high-titer stocks of recombinant adenovirus were generated by two sequential rounds of $CsCl_2$ banding and desalted by gel filtration in Tris-buffered saline on a Sephadex G-50 column. Viral titers were measured by determining the optical densities at 280 nm (OD_{280}) of our viral preparations ($OD_{280} \times 10^{12}$ = viral particles/ml) and checked by plaque assays on 293 cells. Multiplicity of infection (MOI) is expressed as PFU per cell. The number of viral particles required to generate 1 plaque was found to be 25 for both viral vectors used. Viral transductions were performed in a medium containing 2% FCS and 1% penicillin-streptomycin for 16 h.

Measurement of ROS. Exponentially growing cells were labeled in vivo for 20 min at 37°C with 10 μM of 2′,7′-dichlorodihydrofluorescein diacetate (DCF-DA), purchased from Molecular Probes. For analysis of DCF-DA staining, cells were harvested in PBS and analyzed for changes in fluorescence intensity in the Fl-1 channel by flow cytometry (Becton Dickinson; FACSCalibur).

Measurement of mitochondrial membrane potential. Mitochondrial membrane polarization was analyzed by the green fluorescent dye JC-1 (Molecular Probes), which accumulates in the mitochondria in a potential-sensitive manner. Inside the mitochondria at high concentrations, red fluorescent J-aggregates are formed, indicated by a fluorescence emission shift from green (527 nm) to red (590 nm). We calculated the mitochondrial membrane potential as a ratio between red- and green-positive cells (590/527-nm ratio), comparing the changes between parental cell lines and MnSOD-overexpressing cells. Control measurements of mitochondrial size and numbers were carried out with the MitoTracker Green dye (Molecular Probes).

RESULTS

Overexpression of MnSOD induces growth retardation and senescence in the colorectal cancer cell line HCT116. To address the role of the superoxide-scavenging enzyme MnSOD as a tumor suppressor in colon cancer, we stably transfected the human colon cancer cell line HCT116 with a pcDNA-MnSOD construct. For further analysis, we selected two clones which overexpressed different levels of MnSOD: the low-overexpressing clone HCT*MnS*9 and the high-overexpressing clone HCT*MnS*17 (Fig. 1A). Densitometric quantification of the MnSOD signal showed 2.5-fold overexpression in clone HCT*MnS*9 and 6-fold overexpression in clone HCT*MnS*17 compared to the parental cell line HCT116 (Fig. 1B).

To address the growth-retarding activity of MnSOD in hu-

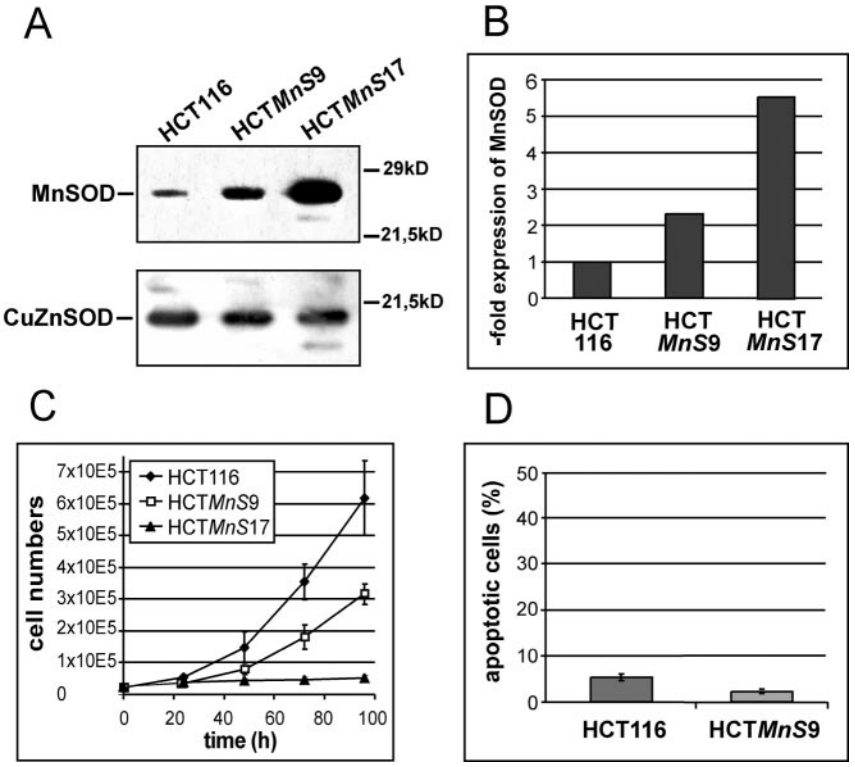

FIG. 1. (A) Western blot analysis of cell lysates from HCT116 and the MnSOD-overexpressing cell lines HCT*MnS*9 and HCT*MnS*17. Membranes were probed with an antibody against MnSOD and with an anti-CuZnSOD antibody (loading control) as indicated. (B) The extent of MnSOD overexpression in the HCT*MnS*9 and HCT*MnS*17 cell lines was measured by densitometric analysis of three different Western blots. In the diagram the overexpression value refers to the parental cell line HCT116. (C) Growth curves of HCT116 and the HCT*MnS*9 and HCT*MnS*17 cell lines. Cell numbers are averages from three independent experiments ± standard errors. (D) Amounts of apoptotic cells in HCT116 and HCT*MnS*9 cells were measured according to a method of Nicoletti et al. (28) in three independent experiments. Results are depicted as means ± standard errors.

man colorectal cancer, we measured the growth of HCT116 and clones HCT*MnS*9 and HCT*MnS*17 over 5 days. Interestingly, with rising MnSOD expression levels, the growth capacity of the cells decreased, indicating a growth-retarding effect of the transgenic protein (Fig. 1C). While the 2.5-fold overexpression in HCT*MnS*9 reduced growth rates by about 50%, the 6-fold overexpression in HCT*MnS*17 nearly abolished growth after 8 passages, leading to a complete loss of the cells after 10 passages. To check whether the reduced cell numbers were due to induction of apoptosis by transgenic MnSOD expression, we performed flow cytometric analysis of propidium iodide-stained cells according to the protocol of Nicoletti et al. (28). Comparison of the cellular sub-G_1 fractions (i.e., apoptotic cells) showed a small decrease in basal apoptosis levels from 5% in HCT116 cells to 2% in the MnSOD-overexpressing clone HCT*MnS*9 (Fig. 1D), demonstrating that apoptosis did not contribute to the observed growth attenuation.

When we compared HCT*MnS*9 and HCT*MnS*17 cells to the parental cell line, we found specific morphological differences. The overexpression of MnSOD in HCT*MnS*17 led to increased cell size and flattening of the cytoplasm (Fig. 2A), a phenotype characteristic of senescent cells. Therefore, we assayed the cells for SA-β-Gal activity. Indeed, we found a senescence-specific enzymatic activity in cells with altered morphology (Fig. 2B). For a direct comparison of senescence in the different MnSOD-overexpressing clones, we embedded stained cells and analyzed the numbers of SA-β-Gal-positive cells (Fig. 2C). In cultures of HCT*MnS*17, significantly more cells were found to be senescent than in HCT*MnS*9 cultures, pointing to a dose dependent induction of cellular senescence by forced overexpression of MnSOD. No staining was observed in HCT116 cells. The quantification of SA-β-Gal-positive cells in the diagram in Fig. 2D shows that in populations of the low-overexpressing clone HCT*MnS*9, about 15% of cells fulfill the criteria of senescence, while in the high-overexpressing cells of HCT*MnS*17, 80% were found to exhibit senescence. This clear correlation between expression levels of the transgenic MnSOD and the degree of senescence supports a role for superoxide radical dismutation in the development of the senescent phenotype.

Measurement of BrdU incorporation is another method to detect senescence and can differentiate between senescence (<5% BrdU positive) and crisis (>30% BrdU positive) based on the number of cells that have actively incorporated BrdU (45). Therefore, we measured BrdU incorporation after a 30-min pulse in HCT*MnS*17 cells in comparison to the parental cell line. In HCT116 we found about 26.1% BrdU-positive cells compared to just 4.2% in HCT*MnS*17 cells (Fig. 2E), confirming that MnSOD overexpression can induce senescence in colorectal cancer cells.

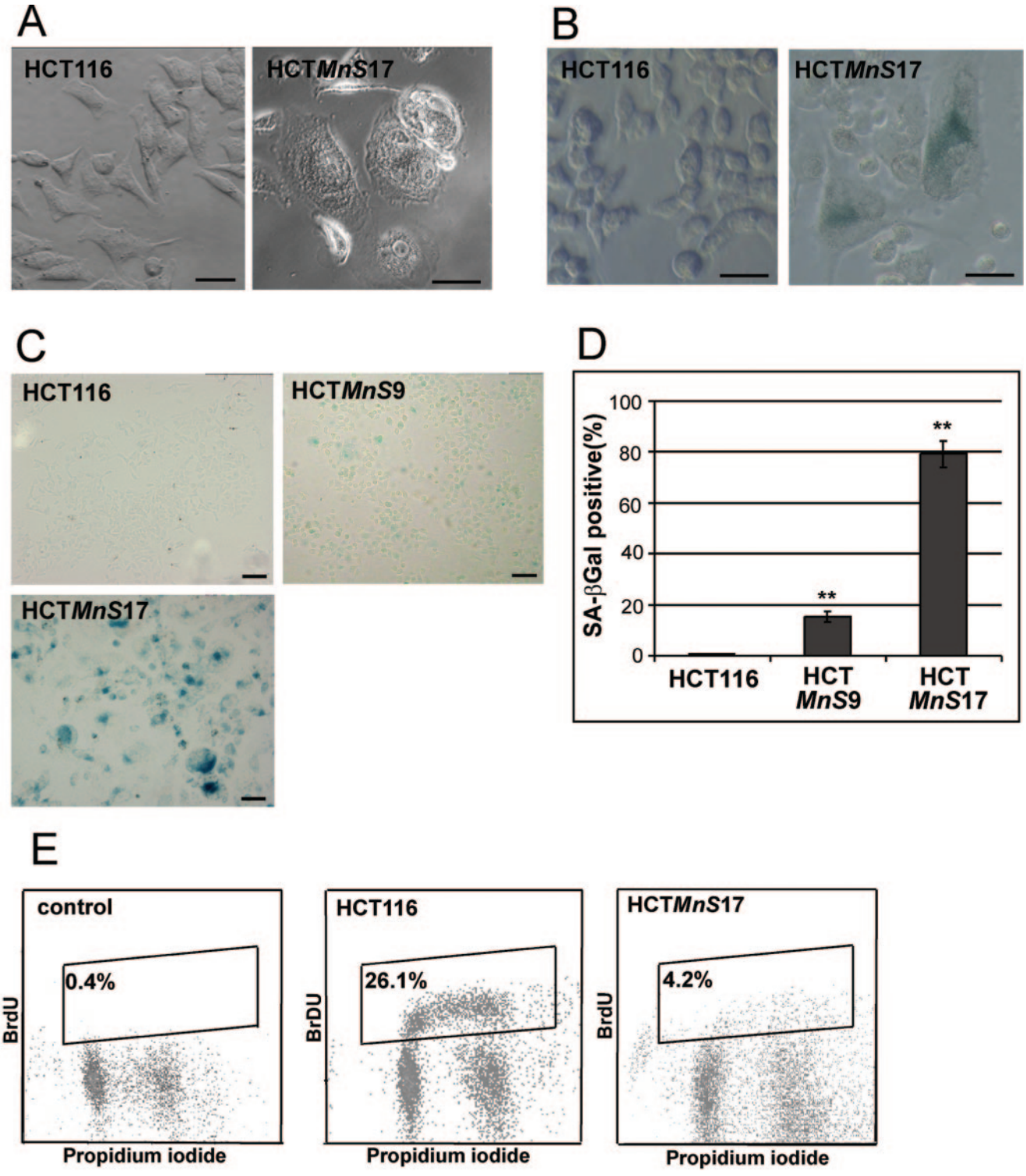

FIG. 2. (A) Microscopic bright-field analysis of the habitus of HCT116 and HCT*MnS*17 cells cultured under normal growth conditions. Bars, 200 μm. (B) Senescence staining of HCT116 and HCT*MnS*17 cells (detail). Cells were stained at pH 6.0 for SA-β-Gal activity according to the method of Dimri and coworkers (9). Pictures in panels A and B were taken on a Zeiss Axiovert 135 inverted microscope with a 40-fold objective. Bars, 200 μm. (C) Comparison of senescence staining of HCT116, HCT*MnS*9, and HCT*MnS*17 cells (overview). Pictures were taken on an upright Olympus BX51 microscope with a 10-fold objective. Bars, 400 μm. (D) Percentages of senescent cells in MnSOD-overexpressing cells. For determination of senescence, 600 cells from three independent SA-β-Gal stainings (± standard errors) were evaluated in microscopic analyses. The significance of differences in senescence between HCT*MnS* clones and HCT116 cells was verified by *t* test analysis. **, $P < 0.001$. (E) The rates of actively replicating cells were measured by incorporation of BrdU into HCT116 and HCT*MnS*17 cells. Diagrams show populations of cells double stained with fluorescein isothiocyanate-labeled BrdU and propidium iodide. The control measurement was performed with propidium iodide-stained HCT116 cells without BrdU staining.

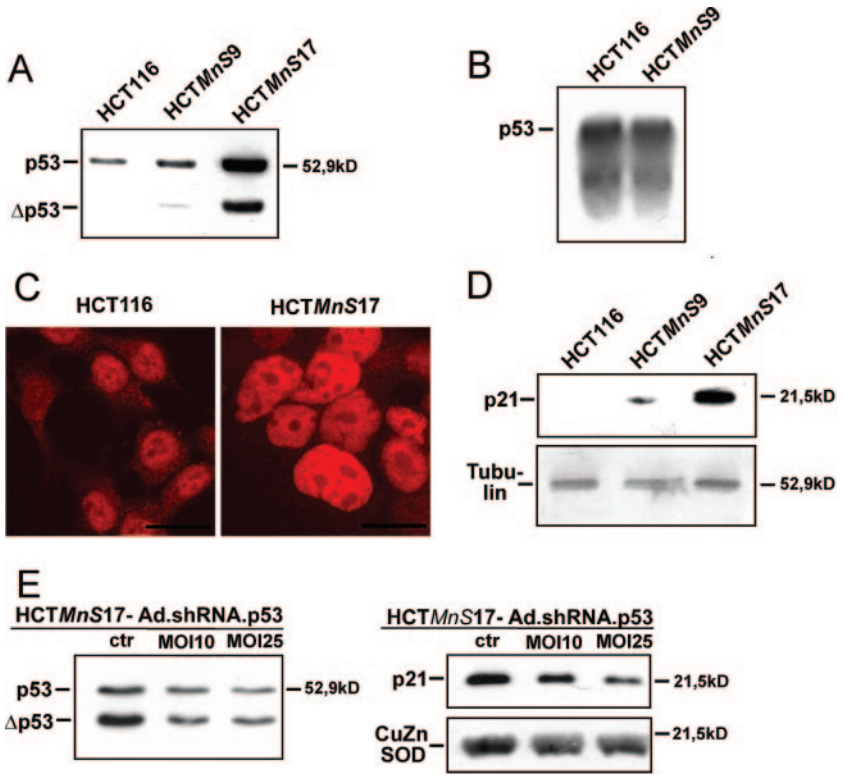

FIG. 3. (A) Comparison of the expression level of p53 in the HCT116 cell line versus the MnSOD-overexpressing cell lines HCT*MnS*9 and HCT*MnS*17 by Western blot analysis. (B) Analysis of mRNA levels of p53 in HCT116 and HCT*MnS*9 cells by Northern blotting. (C) Immunofluorescence analysis of the subcellular localization of p53 in HCT116 and HCT*MnS*17 cells. Bars, 200 μM. (D) Analysis of expression levels of the p53 target gene p21. The expression level of p21 in HCT116 cells was compared to those in the MnSOD-overexpressing cell lines HCT*MnS*9 and HCT*MnS*17 by Western blotting. Western blot analysis of tubulin indicates that equal amounts of protein were loaded for immunodetection in panels A and D. (E) An adenovirally expressed shRNA directed at p53 (Ad.shRNA.p53) can shift the amount of the tumor suppressor protein p53 in HCT*MnS*17 cells back to normal. An adenovirus vector (MOI, 25) expressing a shRNA targeting the jellyfish protein EGFP (Ad.shRNA.EGFP) was used as a control (ctr). Compared to this control, infection at an MOI of 25 reduces the level of p53 back to normal (left) and, in addition, reduces the amount of the transcriptional target p21 (right). The amounts of protein loaded were identical, as indicated by the control Western blot (CuZnSOD).

Induction of cellular senescence by MnSOD is accompanied by a dose-dependent up-regulation of the tumor suppressor p53 and its transcriptional target p21. In order to explore mechanisms that are related to attenuated tumor cell growth as a result of overexpression of MnSOD, we investigated the tumor suppressor p53, a regulator of cell growth, which has been associated with a senescent phenotype in fibroblasts (12, 36). Western blot analysis clearly showed an up-regulation in HCT*MnS*9 cells and a strong increase of p53 in HCT*MnS*17 cells, pointing to an MnSOD dose-dependent up-regulation of the tumor suppressor protein (Fig. 3A). In addition, a p53 delta variant (Δp53) of approximately 42 kDa became apparent in clones overexpressing MnSOD. In order to explore whether increased p53 protein levels were due to up-regulated transcription or higher protein stability, we carried out Northern blot analysis using a p53-specific probe. Comparison of the levels of p53 mRNA showed no difference between HCT116 and HCT*MnS*9 cells, indicating stabilization of p53 at the protein level (Fig. 3B). Since the transcriptional activity of p53 is dependent on its nuclear localization, we compared the subcellular localization of p53 in MnSOD transgenic cells with that in the parental cell line HCT116 by immunofluorescence (Fig. 3C). Even though we detected p53 in the nuclei of HCT116 cells, considerable quantities of p53 were also found in the cytoplasm. Strikingly, in HCT116 cells overexpressing MnSOD, p53 was exclusively present in the nucleus, without any p53-specific staining in the cytoplasm. This nuclear accumulation points to an elevated transactivating activity of p53, potentially giving rise to a consequent up-regulation of its target genes.

A major p53 target is the cyclin-dependent kinase inhibitor p21, which controls entry into the G_1-phase of the cell cycle (11). While p21 is hardly detectable in HCT116 cells, p21 expression is induced in HCT*MnS*9 and to a much greater extent in HCT*MnS*17 (Fig. 3D). In order to test whether this dose-dependent up-regulation of p21 is indeed p53 dependent, we directed a knockdown approach at p53. To this end, we used the adenovirus vector Ad.shRNA.p53, which expresses a shRNA based on a p53 RNAi motif described by Brummelkamp and colleagues (1) from the human RNA polymerase III promoter U6. Using an MOI of 25, we could revert p53 levels in HCT*MnS*17 cells back to wild-type levels (Fig. 3E), which in turn led to a decrease in p21 levels, indicating that p21 up-regulation is dependent on p53. Since both p53 and p21 have been implicated in senescence, we wanted to know which

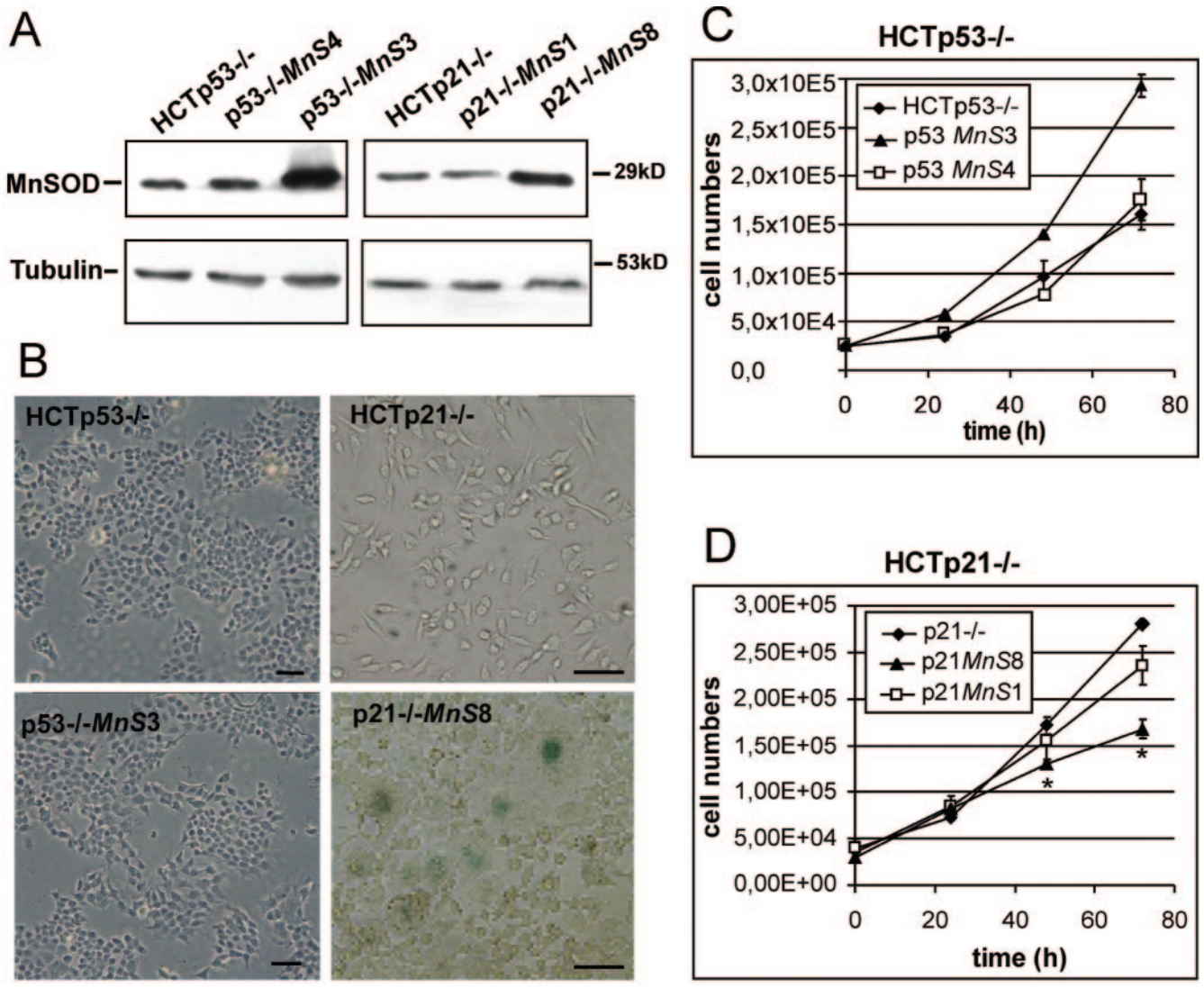

FIG. 4. (A) Expression levels of MnSOD in the parental cell lines HCTp53$^{-/-}$ and HCTp21$^{-/-}$ and in the MnSOD-overexpressing cell lines p53$^{-/-}$*MnS*4 and p53$^{-/-}$*MnS*3 as well as p21$^{-/-}$*MnS*1 and p21$^{-/-}$*MnS*8 analyzed by Western blotting. Immunodetection of tubulin shows equal amounts of protein for all samples. (B) SA-β-Gal activities in HCTp53$^{-/-}$ and HCTp21$^{-/-}$ cells and in the corresponding MnSOD-overexpressing cell lines p53$^{-/-}$*MnS*3 and p21$^{-/-}$*MnS*8. Bars, 250 μm. (C and D) Influence of the overexpression of MnSOD on the growth behavior of p53-negative (C) and p21$^{-/-}$ (D) cells. Cell numbers were determined in three independent experiments. Error bars, standard errors. Asterisks indicate significant differences in cell numbers between MnSOD-overexpressing cells and the parental cell lines. The statistical analysis was performed by *t* test ($P < 0.05$).

factors are required in MnSOD-induced senescence in HCT116 human colorectal cancer cells.

MnSOD-induced cellular senescence depends on p53 but not on p21. To clarify the role of p53 and p21 in MnSOD-induced senescence, we used isogenic knockout cells of p53 (HCTp53$^{-/-}$) and p21 (HCTp21$^{-/-}$), respectively, which were produced by targeted homologous recombination from HCT116 cells (2). We then stably transfected MnSOD, creating the p53-negative cell lines p53$^{-/-}$*MnS*3 and p53$^{-/-}$*MnS*4 as well as the p21-negative cell lines p21$^{-/-}$*MnS*1 and p21$^{-/-}$*MnS*8. Western blot analysis demonstrated that, while clones p53$^{-/-}$*MnS*4 and p21$^{-/-}$*MnS*1 showed very low overexpression of MnSOD, p53$^{-/-}$*MnS*3 and p21$^{-/-}$*MnS*8 showed high levels of overexpression (Fig. 4A). Densitometric determination from three different blots revealed 4.2-fold and 2.7-fold overexpression for p53$^{-/-}$*MnS*3 and p21$^{-/-}$*MnS*8, respectively. To detect senescence, we stained for SA-β-Gal. Neither p53$^{-/-}$*MnS* clone showed signs of senescence, demonstrating that p53 is needed for the induction of senescence by MnSOD. In the p21$^{-/-}$*MnS*8 cell line, we clearly found evidence of cellular senescence by flattened morphology and SA-β-Gal activity in some of the cells (Fig. 4B). Therefore, even though it is up-regulated in MnSOD-overexpressing HCT116 cells, p21 is not essential for senescence in these cells, though we cannot rule out a promoting role of p21 in this process.

We analyzed p53$^{-/-}$ and p21$^{-/-}$ MnSOD-overexpressing cell lines for their growth behaviors. Interestingly, we found that the highly MnSOD overexpressing clone p53$^{-/-}$*MnS*3

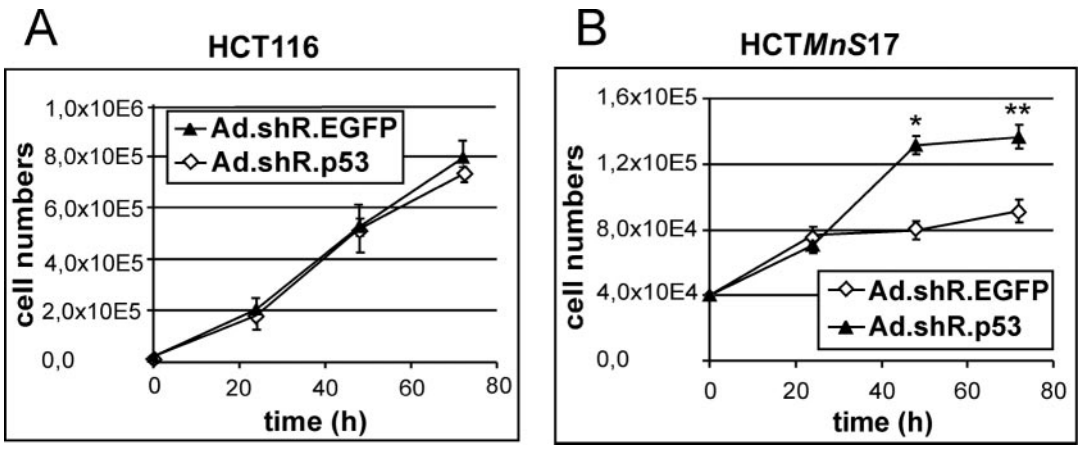

FIG. 5. Growth curves of HCT116 (A) and the MnSOD-overexpressing cell line HCT*MnS*17 (B) infected at an MOI of 25 with Ad.shRNA.p53 or the control vector Ad.shRNA.EGFP. Results are depicted as means; error bars, standard errors. The significance of the growth-stimulatory effect of p53 knockdown in HCT*MnS*17 cells was verified by *t* test analysis. *, $P < 0.05$; **, $P < 0.001$.

showed a slightly enhanced cell growth capacity, while the low-overexpressing clone p53$^{-/-}$*MnS*4 showed growth behavior equivalent to that of the parental cell line HCTp53$^{-/-}$ (Fig. 4C). In contrast, in the senescence-competent HCTp21$^{-/-}$ cells, overexpression of MnSOD led to growth retardation (Fig. 4D) similar to the effects observed in HCT*MnS* clones. While the low-MnSOD-overexpressing cell line p21$^{-/-}$*MnS*1 showed only a small decrease in cell growth, p21$^{-/-}$*MnS*8 cells were about 50% growth inhibited relative to the parental HCTp21$^{-/-}$ cells. Additional HCTp53$^{-/-}$ and HCTp21$^{-/-}$ MnSOD-overexpressing clones showed growth retardation and senescence results similar to those of the clones described above (data not shown). To evaluate the essential role of p53 as an inducer of growth retardation and senescence triggered by MnSOD overexpression, we again took advantage of the adenovirus construct Ad.shRNA.p53. Using this knockdown tool, we measured growth curves of HCT116 and HCT*MnS*17 to examine the role of p53 in MnSOD-related growth suppression. For HCT116 cells we were not able to detect differences in growth behavior by comparing Ad.shRNA.p53-transduced cells to control cells transduced with Ad.shRNA.EGFP (Fig. 5A). However, in HCT*MnS*17 cells, the knockdown of p53 protein by RNA interference led to a significant restoration of growth potential relative to the control (Fig. 5B), once more demonstrating a role for p53 in the growth-retarding activity of MnSOD.

MnSOD reduces the MMP. Excessive H_2O_2 production by MnSOD is one potential explanation for the observed phenotypes. Therefore, we stained cells with DCF-DA, a redox-sensitive dye commonly used to detect the oxidative activity of cells. We compared parental cell lines with MnSOD-overexpressing cell lines by overlaying fluorescent signal peaks in histograms of the Fl-1 channel. We found small increases in fluorescence intensity in both HCT*MnS*9 (Fig. 6A, left) and p53$^{-/-}$*MnS*3 (Fig. 6A, middle) cells. As a control for the sensitivity of the DCF-DA-based measurement of cellular redox status, we compared starved to serum-stimulated HCT116 cells (Fig. 6A, right). As expected, we found a marked increase of oxidative potential in the serum-stimulated cells. In comparison, MnSOD overexpression does not substantially alter the overall redox status of HCT116 colorectal cancer cells, leaving changes of redox status as unlikely causes of the senescence phenotype.

Kim and coworkers (17) have reported that MnSOD can give rise to depolarization across the mitochondrial membrane, a phenomenon that has also been implicated in the development of senescence (49). Therefore, we measured the MMP in our cells. We analyzed the fluorescence of cells that were loaded with the dual-emission probe JC-1. JC-1 specifically senses the MMP by shifting from a monomeric state emitting a green fluorescent signal at a low MMP (emission at 527 nm) into J-aggregates residing in the mitochondrial matrix that give off a red fluorescent light at higher (normal) MMPs (emission maximum, 590 nm). We compared the MMPs of HCT116 and HCTp53$^{-/-}$ with those of their MnSOD-overexpressing counterparts by calculation of 590/527-nm ratios. The ratios were reduced from a value of approximately 1 in the parental cell lines to around 0.4 in both MnSOD-overexpressing cell lines regardless of the p53 status (Fig. 6B). These results clearly demonstrate a reduction in the mitochondrial transmembrane potential by overexpression of MnSOD. To verify that changes in the JC-1 fluorescence signals were not due to changes in the number of mitochondria or their volume, we tested the effect of MnSOD overexpression on the fluorescence uptake of the redox-insensitive mitochondrial dye MitoTracker Green (Fig. 6C). Here we found no evidence for a shift in fluorescence intensity in MnSOD-overexpressing cells, ruling out the possibility of MnSOD-triggered neogenesis of mitochondria or an increase in their size.

Mitochondrial membrane uncoupling leads to activation of p53 and to p53-induced senescence in colorectal cancer. To test the hypothesis that mitochondrial membrane depolarization can initiate a cascade that activates p53, eventually leading to senescence, we used chemical substances known to inhibit the mitochondrial electron transport system (ETS), leading to a reduction in the MMP due to decreased proton-pumping activity. We treated HCT116 cells with the ETS complex I inhibitor ROT and the complex III-inhibiting reagent AA and assayed for p53 by Western blot analysis. Though with different kinetics, both reagents induced activation of p53. ROT in-

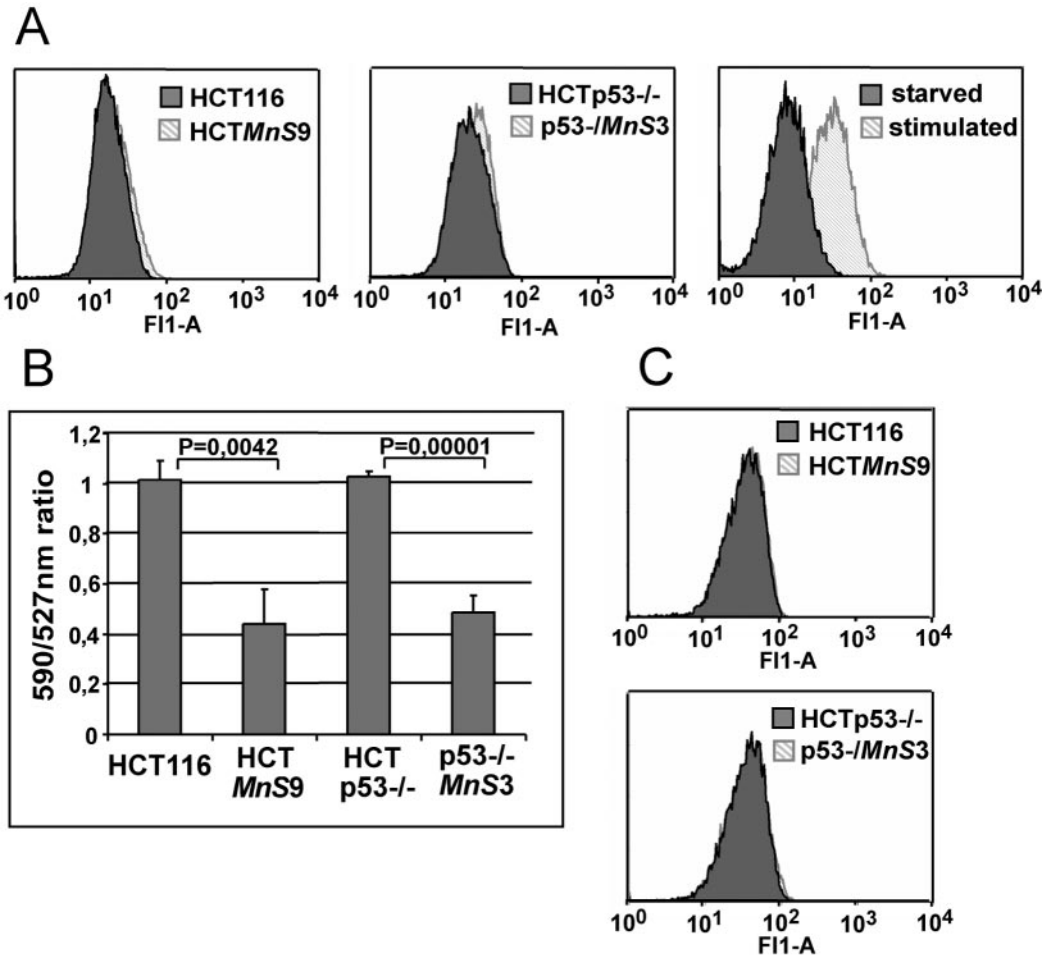

FIG. 6. (A) Measurement of cellular oxidative activity with the redox-sensitive dye DCF-DA. Labeled cells were analyzed by flow cytometry in the Fl-1 channel. The histogram of the parental cell line HCT116 or HCTp53$^{-/-}$ (dark gray) is overlaid with the histogram of the corresponding MnSOD-overexpressing cell line (light gray). As controls (right), cells were either grown in serum-free medium for 6 h before labeling (dark gray) or serum starved for 24 h and subsequently stimulated for 6 h with McCoy's medium containing 20% FCS (light gray). (B) MMP was detected by the emission intensity of the dual fluorescent potential-sensitive dye JC-1. JC-1-labeled cells were analyzed by flow cytometry for their emissions at wavelengths of 527 nm (Fl-1 channel) and 590 nm (Fl-2 channel). The 590/527-nm ratio, which is a function of the electrochemical gradient of the inner mitochondrial membrane, was calculated. To compare the MnSOD-overexpressing with the parental cell lines, the 590/527-nm ratio of parental cells was set to 1. Ratios are means from three experiments ± standard errors. (C) Mitochondrial mass was analyzed by use of the mitochondrial dye MitoTracker Green. Cells were stained with the redox-insensitive living dye MitoTracker Green and analyzed in the Fl-1 channel of a flow cytometer. Parental (dark gray) and MnSOD-overexpressing (light gray) cells were compared in a histogram overlay.

duced p53 expression with a maximal expression level at 48 h, while after AA treatment, p53 levels peaked at 24 h (Fig. 7A). These results point to a general mechanism that leads from a reduction of MMP to increased p53 activity. To validate the finding that under the chosen experimental conditions the MMP is reduced by both ETS inhibitors, we investigated the JC-1 emission profiles. In HCT116 cells treated with either ROT or AA, we found a marked fluorescence shift as indicated by the decrease in the 590/527-nm ratio (Fig. 7B), confirming the potency of both substances to reduce MMP.

We asked whether uncoupling substrates also have the potential to induce senescence in colorectal cancer cells. We treated HCT116 and HCTp53$^{-/-}$ cells with either ROT or AA for as long as 7 days and assayed these cells for SA-β-Gal activity. Both uncoupling reagents were capable of inducing senescence in HCT116 cells (Fig. 7C, top panels). In HCTp53$^{-/-}$ cells treated with ROT (Fig. 7C, lower left) or AA (Fig. 7C, lower right), SA-β-Gal staining above background levels could not be detected. These results indicate that the reduction of MMP by inhibitors of the ETS, in analogy to MnSOD, can guide cells into p53-dependent senescence.

Because loss of MMP by mitochondrial inhibitors is often linked to ROS production, we analyzed the oxidative status of DCF-DA-stained ROT- and AA-treated cells by flow cytometry. In the overlay of treated versus untreated cells, it becomes apparent that only AA, not ROT, is an inducer of ROS in HCT116 cells (Fig. 7D). These results are in line with the observations of Chen and coworkers (6), which showed ROS production from mitochondria by AA but not by ROT treatment. Our data indicate that loss of MMP, which is the common feature of both drugs, not excessive free radical/H_2O_2 production, is the major inducer of senescence in these cells.

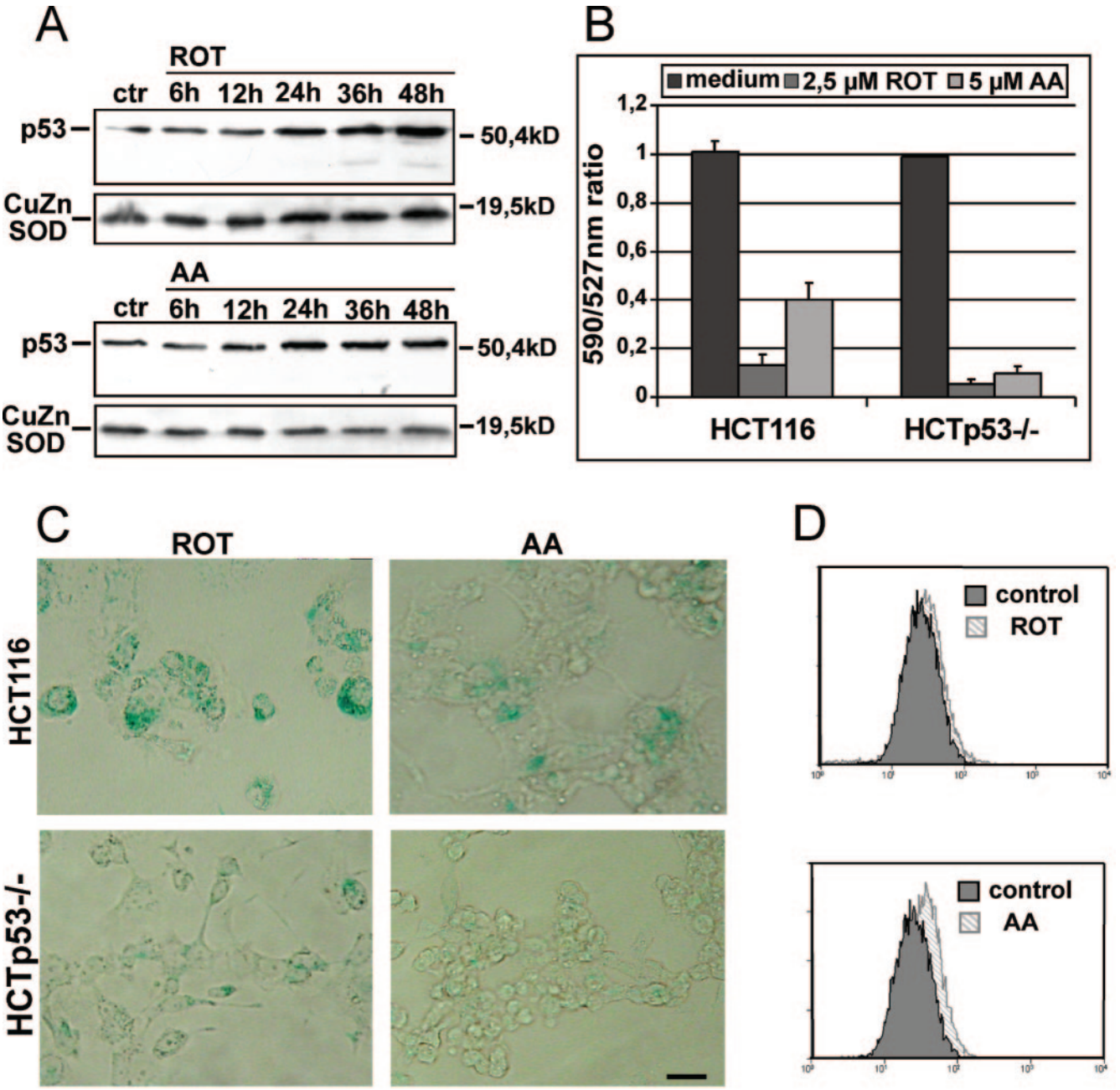

FIG. 7. (A) Time course of p53 expression levels of HCT116 cells treated with the ETS inhibitor ROT or AA. HCT116 cells were treated for the indicated times with 2.5 μM ROT or 5 μM AA and analyzed by Western blotting. As loading controls, Western blots were probed with an antibody against CuZnSOD. (B) 590/527-nm ratios of JC-1 stained HCT116 and HCTp53$^{-/-}$ cells treated with either ROT or AA. Cells were treated with 2.5 μM ROT or 5 μM AA for 30 min in the presence of JC-1. The 590/527-nm ratios of treated cells were compared to that of untreated cells, for which the ratio was set to 1. Results are means from two independent experiments. Error bars, standard errors. (C) SA-β-Gal activities of HCT116 and HCTp53$^{-/-}$ cells treated with ROT or AA. After treatment for 6 days with 2.5 μM ROT or 5 μM AA, cells were fixed and stained for SA-β-Gal activity. Pictures were taken at a magnification of ×200. Bar, 100 μm. (D) Flow cytometric analysis of HCT116 cells stained with DCF-DA. The histograms show overlaps of 2.5 μM ROT- or 5 μM AA-treated cells (light gray) with untreated control cells (dark gray).

DISCUSSION

Several studies have shown that overexpressed MnSOD suppresses growth of tumor cells from various human malignancies including breast cancer (22), melanoma (7), and glioma (51). Based on this growth-retarding effect, it has been hypothesized that MnSOD might be a tumor suppressor gene and that restoring MnSOD activity should reverse the malignant phenotype of tumor cells (30). On the basis of growth curves and colony-forming assays (data not shown), we confirmed that in the colon cancer cell line HCT116, growth can be increasingly reduced by rising levels of MnSOD. However, to date no good mechanism has been proposed by which MnSOD may influ-

ence cellular growth behavior. We show that the tumor suppressor p53 is required for growth suppression by MnSOD. In this context we found that p53 was stabilized at the protein level and accumulated in the nuclei of MnSOD-overexpressing cells. In addition, with the antibody DO-1, which maps to an N-terminal epitope of p53, we detected a presumably C-terminally truncated delta variant of p53 (Δp53) that is specific for MnSOD-overexpressing clones. A similar Δp53 has been linked to stress responses in colorectal cancer cells, since it has been found in lysates of 5-fluorouracil-treated HCT116 cells (Andrea Mohr, personal communication). Furthermore, when we knocked down p53 by RNAi in MnSOD-overexpressing cells, we restored growth in these cells, demonstrating the requirement for p53 in MnSOD-mediated growth suppression and senescence.

We also found the p53 target gene p21 up-regulated in a dose dependent fashion in MnSOD-overexpressing cells. With DNA-directed RNAi against p53, we were able to reduce the amount of p21, indicating direct signaling of MnSOD overexpression through p53 onto p21. The p53 protein has been shown to control the cell cycle at the G_1/S boundary through p21 (11). In addition, p53 is able to control the G_2 checkpoint through the activation of both p21 and 14-3-3σ (2, 13). However, we found growth suppression and senescence in $p21^{-/-}$ cells overexpressing MnSOD, demonstrating that p21 is not necessary for the antiproliferative effects, at least in the cell system examined. Nevertheless, p21 has often been implicated in senescence. Macip and coworkers (25) reported that p21-induced senescence requires ROS formation, since chemical scavengers could prevent p21-mediated senescence induction. Since we could not find elevated ROS levels in MnSOD-overexpressing cells, p21 might not be of essential importance in our senescence model. Furthermore, our results are in line with a report that failed to establish a role of p21 in cooperative senescence induction by p53 and oncogenic Ras (5), possibly resembling the situation in MnSOD-overexpressing HCT116 and HCT$p21^{-/-}$ cells.

In vivo the function of tumor suppressors largely depends on their ability to trigger senescence (34). Intriguingly, a transgenic mouse which carries an activated p53 shows an early-aging phenotype and enhanced tumor resistance, consistent with the idea that p53 controls senescence as a mechanism of tumor suppression (44). Furthermore, $p53^{-/-}$ mice develop spontaneous malignancies, while p21 knockout mice have no increased tumor susceptibility (10, 38). These differences demonstrate that the in vivo tumor suppressor function of p53 is not mediated by p21 and does not depend on cell cycle control in G_1 as mediated by p21. In this regard our data indicating no decisive role for p21 in senescence induction may reflect the in vivo situation in mice. Thus, it is possible that the role of p21 in senescence is restricted to replicative senescence of primary cells.

Depending on the cell type, other p53-cooperating factors have been implicated in senescence. In contrast to results that emphasize the important role of the INK4a system in drug-induced premature senescence of murine lymphomas (35), the HCT116 cell system used in our study is deficient in $p14^{ARF}$ as well as $p16^{INK4A}$ due to promoter methylation and a frameshift mutation (3). We confirmed these results by Western blot analysis (data not shown). Therefore, in premature senescence, cell type-specific differences might exist, which require different combinations of tumor suppressors or activated signaling pathways. In the colon cancer cell line HCT116 used in this study, K-Ras activation plays a key-role in the transformed phenotype (39). In primary fibroblasts it has been shown that the cooperative activation of Ras and p53 leads to replicative senescence (5, 12, 36). Therefore, it is believed that for cells to tolerate activating Ras mutations, they require the parallel inactivation of p53, which is exactly what is found in most colon cancer cells. HCT116 cells possess activating K-Ras mutations and wild-type p53, with the latter, however, being partially restrained in its activity by mutations in downstream effectors such as $p14^{ARF}$. In nonactivated HCT116 cells, the loss of $p14^{ARF}$ might explain the loss of tumor suppressor functions of p53. By overexpression of MnSOD, p53 becomes activated and might be capable of circumventing blocks caused by mutations and silencing events, thereby switching on dormant pathways downstream of the mutational hurdle. This scenario might explain how the tumor suppressor function of p53 can be "reactivated" in HCT*MnS* cells.

Despite its general tumor suppressor activity, MnSOD has also given rise to a number of conflicting reports with regard to its expression level in different tumors. It was shown that MnSOD expression positively correlates with tumor grade in malignant melanoma (33), breast carcinoma (43), and colorectal carcinoma (29) and, in addition, with the invasive and metastatic phenotype of tumors (8, 26). On a molecular level, MnSOD overexpression can activate matrix metalloproteases, which are implicated in cell migration and invasiveness (46, 50). This discrepancy between growth inhibition on the one hand and the association with malignancy on the other hand might be explained with the help of the tumor progression model for colorectal cancer suggested by Kinzler and Vogelstein (18). In this sequence of genetic changes, adenomatoos polyposis coli mutations initiate neoplastic progress, followed by the gain of K-Ras and the eventual mutational loss of p53 function. In low-grade tumors with predominantly functional p53, MnSOD levels are often found to be low. We suggest that overexpression of MnSOD at this relatively early stage of tumor progression could be of therapeutic benefit, since high levels of MnSOD would result in growth arrest by senescence. As tumor progression proceeds, p53 becomes inactivated, leading to an increasing loss of growth control. At this point the outcome of MnSOD expression may change. High levels of MnSOD, no longer able to induce senescence and growth control due to the lack of p53, might be one of the driving forces behind the invasive phenotype of high-grade tumors by promoting the activity of a number of matrix-rebuilding enzymes. Consequently, our observation that MnSOD overexpression in p53-negative cells had no negative influence on cell proliferation, while it repressed growth in p53-competent cells, may offer a rationale for the opposing data concerning the influence of MnSOD in tumorigenic processes.

A striking observation of our study is that MnSOD overexpression reduces the MMP, which has been reported before by Kim and colleagues (17). Furthermore, we established that MnSOD-induced MMP loss is p53 independent. Therefore, we hypothesize that decreased MMP might work as a trigger for senescence upstream of p53. Interestingly, MMP reduction has been found in organismal aging (32, 40), and defects in mito-

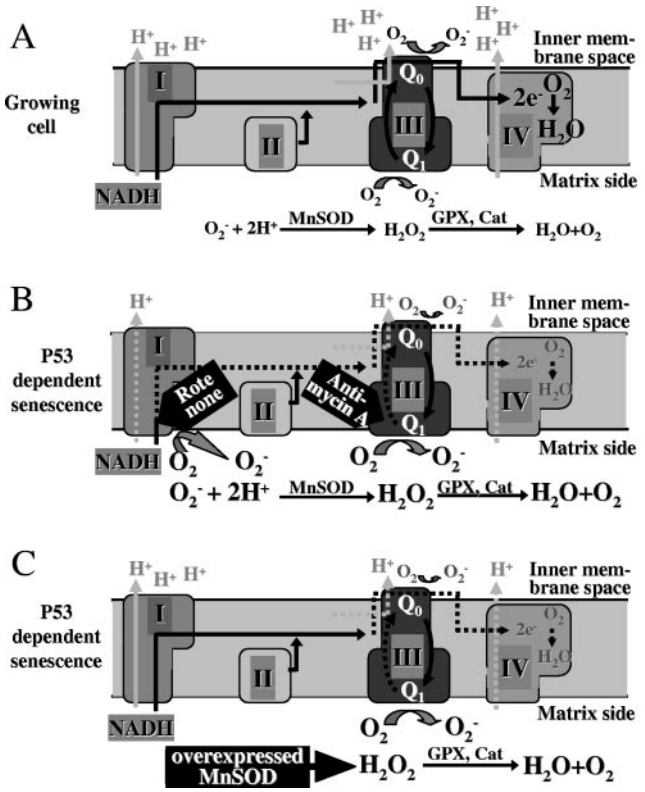

FIG. 8. Model for the reduction of MMP by MnSOD overexpression. MnSOD acts as an electron trap on the matrix side. (A) Mechanistic view of the electron transport chain of the inner mitochondrial membrane of normally growing cells. Electrons are transported from reduced substrates (such as NADH) along the complexes of the respiratory chain of the inner mitochondrial membrane onto oxygen in complex IV. By simultaneous transport of protons from the matrix to the inner membrane space, an electrochemical force is generated called mitochondrial membrane potential, which drives ATP synthesis. As by-products, electrons are transferred onto oxygen primarily at the level of complex III, leading to superoxide radical production in the inner membrane space (from the cytochrome Q_0 site) and at the matrix side (cytochrome Q_1 site). The enzymes of the antioxidant defense system in the mitochondrial matrix, such as MnSOD, catalase (Cat), and glutathione peroxidases (GPX), detoxify superoxide radicals to water and oxygen. (B) Uncoupling of electron transport by ROT at the level of complex I or by AA at the level of complex III generates increased amounts of electrons at the matrix side of the mitochondrion, which leads to enhanced matrix and reduced cytosolic superoxide production. The dysfunctional electron transport impairs the proton transport, which diminishes the MMP. (C) We assume that loss of MMP is also induced by MnSOD overexpression via intensified electron consumption in the matrix of the mitochondrion. Presumably, at the Q_1 site of complex III, electrons flow into the increased dismutation reaction catalyzed by elevated levels of MnSOD. Because of the reduced electron flow to the inner membrane space, cytosolic superoxide levels are reduced. Consequently, MnSOD acts as a kind of electron trap on the mitochondrial matrix side, which redirects further electrons to the matrix side, thereby increasing the production of hydrogen peroxide, which is detoxified by GPX and Cat, eventually leading to a lack of electrons and to membrane depolarization.

chondrial electron transport are known to induce senescence-associated growth arrest (49). However, loss of MMP and generation of ROS are closely linked processes. Although we were not able to detect major changes in the cellular oxidative status of MnSOD-overexpressing and ROT-treated cells, we cannot completely rule out a contribution of free radicals in senescence induction in HCT116 cells.

Functional cross talk between MnSOD and constituents of the electron transport chain might be of physiological relevance. The generation of superoxide anions on the mitochondrial matrix side occurs even under normal conditions by accidental transfer of electrons onto molecular oxygen. MnSOD detoxifies these reactive oxygen species. When MnSOD is overexpressed, more and more superoxide radicals are converted to H_2O_2 and are thereby pulled out of the physiological equilibrium, resulting in increased production of superoxide and functional loss of electrons from the ETS. This electron consumption on the matrix side might compete with the normal electron transfer onto oxygen, which is required for the buildup of the electrochemical proton gradient, which consequently drives oxidative phosphorylation. A decrease of the proton gradient constitutes a reduction of the MMP. A mechanistic view of the molecular events that are possibly initiated by MnSOD at the level of the electron transport chain is depicted in Fig. 8.

Our model might provide a explanation for the growth inhibition by forced MnSOD expression observed in several tumor cells in vitro and in vivo (7, 22, 51). It remains to be clarified whether MnSOD requires the presence of oncogenic Ras and whether it is capable of inducing senescence in cells which harbor specific p53 point mutations, the first and foremost cause of p53 activity loss in cancer. Evaluating those mutated forms of p53 that retain partial functions will be of special interest. Pharmacological or gene therapeutic targeting of this pathway and reinitiation of aging and subsequent senescence in transformed cells could become a new concept for the treatment of cancer. However, the elucidation of the "senescence pathways" is an indispensable prerequisite for the development of such approaches.

ACKNOWLEDGMENTS

The work was initiated at the University of Edinburgh, Department of Oncology. We thank B. Vogelstein for providing us with the colorectal cancer cell lines HCT116, HCTp53$^{-/-}$, and HCTp21$^{-/-}$. Furthermore, we are grateful to K. Fisher for assistance with RNAi vectors, and we thank S. Kochanek and F. Kreppel for practical help with virus production. In addition, we thank S. Kochanek and A. Presente for carefully reading the manuscript. We thank K. Scharffetter-Kochanek and B. Baumann for reagents and S. Thimm for technical help.

This work was supported by an Emmy-Noether grant from the Deutsche Forschungsgemeinschaft (Zw60/2-1).

REFERENCES

1. **Brummelkamp, T. R., R. Bernards, and R. Agami.** 2002. A system for stable expression of short interfering RNAs in mammalian cells. Science **296:**550–553.
2. **Bunz, F., A. Dutriaux, C. Lengauer, T. Waldman, S. Zhou, J. P. Brown, J. M. Sedivy, K. W. Kinzler, and B. Vogelstein.** 1998. Requirement for p53 and p21 to sustain G_2 arrest after DNA damage. Science **282:**1497–1501.
3. **Burri, N., P. Shaw, H. Bouzourene, I. Sordat, B. Sordat, M. Gillet, D. Schorderet, F. T. Bosman, and P. Chaubert.** 2001. Methylation silencing and mutations of the p14ARF and p16^{INK4a} genes in colon cancer. Lab. Investig. **81:**217–229.
4. **Campisi, J.** 2001. Cellular senescence as a tumor-suppressor mechanism. Trends Cell Biol. **11:**S27–S31.
5. **Castro, M. E., G. M. del Valle, V. Moneo, and A. Carnero.** 2004. Cellular senescence induced by p53-ras cooperation is independent of p21waf1 in murine embryo fibroblasts. J. Cell. Biochem. **92:**514–524.
6. **Chen, Q., E. J. Vazquez, S. Moghaddas, C. L. Hoppel, and E. J. Lesnefsky.** 2003. Production of reactive oxygen species by mitochondria: central role of complex III. J. Biol. Chem. **278:**36027–36031.

7. **Church, S. L., J. W. Grant, L. A. Ridnour, L. W. Oberley, P. E. Swanson, P. S. Meltzer, and J. M. Trent.** 1993. Increased manganese superoxide dismutase expression suppresses the malignant phenotype of human melanoma cells. Proc. Natl. Acad. Sci. USA **90:**3113–3117.
8. **Cullen, J. J., C. Weydert, M. M. Hinkhouse, J. Ritchie, F. E. Domann, D. Spitz, and L. W. Oberley.** 2003. The role of manganese superoxide dismutase in the growth of pancreatic adenocarcinoma. Cancer Res. **63:**1297–1303.
9. **Dimri, G. P., X. Lee, G. Basile, M. Acosta, G. Scott, C. Roskelley, E. E. Medrano, M. Linskens, I. Rubelj, O. Pereira-Smith, et al.** 1995. A biomarker that identifies senescent human cells in culture and in aging skin in vivo. Proc. Natl. Acad. Sci. USA **92:**9363–9367.
10. **Donehower, L. A., M. Harvey, B. L. Slagle, M. J. McArthur, C. A. Montgomery, Jr., J. S. Butel, and A. Bradley.** 1992. Mice deficient for p53 are developmentally normal but susceptible to spontaneous tumours. Nature **356:**215–221.
11. **el Deiry, W. S., T. Tokino, V. E. Velculescu, D. B. Levy, R. Parsons, J. M. Trent, D. Lin, W. E. Mercer, K. W. Kinzler, and B. Vogelstein.** 1993. WAF1, a potential mediator of p53 tumor suppression. Cell **75:**817–825.
12. **Ferbeyre, G., E. de Stanchina, A. W. Lin, E. Querido, M. E. McCurrach, G. J. Hannon, and S. W. Lowe.** 2002. Oncogenic ras and p53 cooperate to induce cellular senescence. Mol. Cell. Biol. **22:**3497–3508.
13. **Hermeking, H., C. Lengauer, K. Polyak, T. C. He, L. Zhang, S. Thiagalingam, K. W. Kinzler, and B. Vogelstein.** 1997. 14-3-3σ is a p53-regulated inhibitor of G_2/M progression. Mol. Cell **1:**3–11.
14. **Horner, S. M., R. A. DeFilippis, L. Manuelidis, and D. DiMaio.** 2004. Repression of the human papillomavirus E6 gene initiates p53-dependent, telomerase-independent senescence and apoptosis in HeLa cervical carcinoma cells. J. Virol. **78:**4063–4073.
15. **Hu, N., A. Gutsmann, D. C. Herbert, A. Bradley, W. H. Lee, and E. Y. Lee.** 1994. Heterozygous Rb-1 delta 20/+ mice are predisposed to tumors of the pituitary gland with a nearly complete penetrance. Oncogene **9:**1021–1027.
16. **Irani, K., Y. Xia, J. L. Zweier, S. J. Sollott, C. J. Der, E. R. Fearon, M. Sundaresan, T. Finkel, and P. J. Goldschmidt-Clermont.** 1997. Mitogenic signaling mediated by oxidants in Ras-transformed fibroblasts. Science **275:** 1649–1652.
17. **Kim, A., W. Zhong, and T. D. Oberley.** 2004. Reversible modulation of cell cycle kinetics in NIH/3T3 mouse fibroblasts by inducible overexpression of mitochondrial manganese superoxide dismutase. Antioxid. Redox. Signal. **6:**489–500.
18. **Kinzler, K. W., and B. Vogelstein.** 1996. Lessons from hereditary colorectal cancer. Cell **87:**159–170.
19. **Krimpenfort, P., K. C. Quon, W. J. Mooi, A. Loonstra, and A. Berns.** 2001. Loss of $p16^{Ink4a}$ confers susceptibility to metastatic melanoma in mice. Nature **413:**83–86.
20. **Lam, E. W., R. Zwacka, J. F. Engelhardt, B. L. Davidson, F. E. Domann, Jr., T. Yan, and L. W. Oberley.** 1997. Adenovirus-mediated manganese superoxide dismutase gene transfer to hamster cheek pouch carcinoma cells. Cancer Res. **57:**5550–5556.
21. **Lam, E. W., R. Zwacka, E. A. Seftor, D. R. Nieva, B. L. Davidson, J. F. Engelhardt, M. J. Hendrix, and L. W. Oberley.** 1999. Effects of antioxidant enzyme overexpression on the invasive phenotype of hamster cheek pouch carcinoma cells. Free Radic. Biol. Med. **27:**572–579.
22. **Li, J. J., L. W. Oberley, D. K. St Clair, L. A. Ridnour, and T. D. Oberley.** 1995. Phenotypic changes induced in human breast cancer cells by overexpression of manganese-containing superoxide dismutase. Oncogene **10:**1989–2000.
23. **Lin, A. W., M. Barradas, J. C. Stone, L. van Aelst, M. Serrano, and S. W. Lowe.** 1998. Premature senescence involving p53 and p16 is activated in response to constitutive MEK/MAPK mitogenic signaling. Genes Dev. **12:** 3008–3019.
24. **Liu, R., T. D. Oberley, and L. W. Oberley.** 1997. Transfection and expression of MnSOD cDNA decreases tumor malignancy of human oral squamous carcinoma SCC-25 cells. Hum. Gene Ther. **8:**585–595.
25. **Macip, S., M. Igarashi, L. Fang, A. Chen, Z. Q. Pan, S. W. Lee, and S. A. Aaronson.** 2002. Inhibition of p21-mediated ROS accumulation can rescue p21-induced senescence. EMBO J. **21:**2180–2188.
26. **Malafa, M., J. Margenthaler, B. Webb, L. Neitzel, and M. Christophersen.** 2000. MnSOD expression is increased in metastatic gastric cancer. J. Surg. Res. **88:**130–134.
27. **Mukhopadhyay-Sardar, S., M. P. Rana, and M. Chatterjee.** 2000. Antioxidant associated chemoprevention by selenomethionine in murine tumor model. Mol. Cell. Biochem. **206:**17–25.
28. **Nicoletti, I., G. Migliorati, M. C. Pagliacci, F. Grignani, and C. Riccardi.** 1991. A rapid and simple method for measuring thymocyte apoptosis by propidium iodide staining and flow cytometry. J. Immunol. Methods **139:** 271–279.
29. **Nozoe, T., M. Honda, S. Inutsuka, M. Yasuda, and D. Korenaga.** 2003. Significance of immunohistochemical expression of manganese superoxide dismutase as a marker of malignant potential in colorectal carcinoma. Oncol. Rep. **10:**39–43.
30. **Oberley, L. W.** 2001. Anticancer therapy by overexpression of superoxide dismutase. Antioxid. Redox. Signal. **3:**461–472.
31. **Psyrri, A., R. A. DeFilippis, A. P. Edwards, K. E. Yates, L. Manuelidis, and D. DiMaio.** 2004. Role of the retinoblastoma pathway in senescence triggered by repression of the human papillomavirus E7 protein in cervical carcinoma cells. Cancer Res. **64:**3079–3086.
32. **Rottenberg, H., and S. Wu.** 1997. Mitochondrial dysfunction in lymphocytes from old mice: enhanced activation of the permeability transition. Biochem. Biophys. Res. Commun. **240:**68–74.
33. **Schadendorf, D., T. Zuberbier, S. Diehl, C. Schadendorf, and B. M. Czarnetzki.** 1995. Serum manganese superoxide dismutase is a new tumour marker for malignant melanoma. Melanoma Res. **5:**351–353.
34. **Schmitt, C. A.** 2003. Senescence, apoptosis and therapy—cutting the lifelines of cancer. Nat. Rev. Cancer **3:**286–295.
35. **Schmitt, C. A., J. S. Fridman, M. Yang, S. Lee, E. Baranov, R. M. Hoffman, and S. W. Lowe.** 2002. A senescence program controlled by p53 and $p16^{INK4a}$ contributes to the outcome of cancer therapy. Cell **109:**335–346.
36. **Serrano, M., A. W. Lin, M. E. McCurrach, D. Beach, and S. W. Lowe.** 1997. Oncogenic ras provokes premature cell senescence associated with accumulation of p53 and $p16^{INK4a}$. Cell **88:**593–602.
37. **Shay, J. W., O. M. Pereira-Smith, and W. E. Wright.** 1991. A role for both RB and p53 in the regulation of human cellular senescence. Exp. Cell Res. **196:**33–39.
38. **Shiohara, M., K. Koike, A. Komiyama, and H. P. Koeffler.** 1997. p21WAF1 mutations and human malignancies. Leuk. Lymphoma **26:**35–41.
39. **Shirasawa, S., M. Furuse, N. Yokoyama, and T. Sasazuki.** 1993. Altered growth of human colon cancer cell lines disrupted at activated Ki-ras. Science **260:**85–88.
40. **Sugrue, M. M., Y. Wang, H. J. Rideout, R. M. Chalmers-Redman, and W. G. Tatton.** 1999. Reduced mitochondrial membrane potential and altered responsiveness of a mitochondrial membrane megachannel in p53-induced senescence. Biochem. Biophys. Res. Commun. **261:**123–130.
41. **te Poele, R. H., A. L. Okorokov, L. Jardine, J. Cummings, and S. P. Joel.** 2002. DNA damage is able to induce senescence in tumor cells in vitro and in vivo. Cancer Res. **62:**1876–1883.
42. **Tremain, R., M. Marko, V. Kinnimulki, H. Ueno, E. Bottinger, and A. Glick.** 2000. Defects in TGF-β signaling overcome senescence of mouse keratinocytes expressing v-Ha-ras. Oncogene **19:**1698–1709.
43. **Tsanou, E., E. Ioachim, E. Briasoulis, K. Damala, A. Charchanti, V. Karavasilis, N. Pavlidis, and N. J. Agnantis.** 2004. Immunohistochemical expression of superoxide dismutase (MnSOD) anti-oxidant enzyme in invasive breast carcinoma. Histol. Histopathol. **19:**807–813.
44. **Tyner, S. D., S. Venkatachalam, J. Choi, S. Jones, N. Ghebranious, H. Igelmann, X. Lu, G. Soron, B. Cooper, C. Brayton, S. Hee Park, T. Thompson, G. Karsenty, A. Bradley, and L. A. Donehower.** 2002. p53 mutant mice that display early ageing-associated phenotypes. Nature **415:**45–53.
45. **Wei, W., and J. M. Sedivy.** 1999. Differentiation between senescence (M1) and crisis (M2) in human fibroblast cultures. Exp. Cell Res. **253:**519–522.
46. **Wenk, J., P. Brenneisen, M. Wlaschek, A. Poswig, K. Briviba, T. D. Oberley, and K. Scharffetter-Kochanek.** 1999. Stable overexpression of manganese superoxide dismutase in mitochondria identifies hydrogen peroxide as a major oxidant in the AP-1-mediated induction of matrix-degrading metalloprotease-1. J. Biol. Chem. **274:**25869–25876.
47. **Xu, H. J., Y. Zhou, W. Ji, G. S. Perng, R. Kruzelock, C. T. Kong, R. C. Bast, G. B. Mills, J. Li, and S. X. Hu.** 1997. Reexpression of the retinoblastoma protein in tumor cells induces senescence and telomerase inhibition. Oncogene **15:**2589–2596.
48. **Yan, T., L. W. Oberley, W. Zhong, and D. K. St Clair.** 1996. Manganese-containing superoxide dismutase overexpression causes phenotypic reversion in SV40-transformed human lung fibroblasts. Cancer Res. **56:**2864–2871.
49. **Yoon, Y. S., H. O. Byun, H. Cho, B. K. Kim, and G. Yoon.** 2003. Complex II defect via down-regulation of iron-sulfur subunit induces mitochondrial dysfunction and cell cycle delay in iron chelation-induced senescence-associated growth arrest. J. Biol. Chem. **278:**51577–51586.
50. **Zhang, H. J., W. Zhao, S. Venkataraman, M. E. Robbins, G. R. Buettner, K. C. Kregel, and L. W. Oberley.** 2002. Activation of matrix metalloproteinase-2 by overexpression of manganese superoxide dismutase in human breast cancer MCF-7 cells involves reactive oxygen species. J. Biol. Chem. **277:** 20919–20926.
51. **Zhong, W., L. W. Oberley, T. D. Oberley, and D. K. St Clair.** 1997. Suppression of the malignant phenotype of human glioma cells by overexpression of manganese superoxide dismutase. Oncogene **14:**481–490.
52. **Zwacka, R. M., W. Zhou, Y. Zhang, C. J. Darby, L. Dudus, J. Halldorson, L. Oberley, and J. F. Engelhardt.** 1998. Redox gene therapy for ischemia/reperfusion injury of the liver reduces AP1 and NF-κB activation. Nat. Med. **4:**698–704.